Supporting Information

Molecular assemblies of the catalytic domain of SOS with KRas and oncogenic mutants

Zahra Moghadamchargari,[1] Mehdi Shirzadeh,[1] Chang Liu,[2] Samantha Schrecke,[1] Charles Packianathan,[1] David H. Russell,[1] Minglei Zhao,[2] Arthur Laganowsky[1,*]

Correspondence to: ALaganowsky@chem.tamu.edu

Methods

Protein expression and purification. The KRas4B (residues 1-169) was expressed and purified as previously described.(1) In brief, the KRas4B (referred to as KRas) expression construct including an N-terminal TEV protease cleavable His_6 tag was transformed into Lemo21-(DE3) *E. coli* (New England Biolabs) and grown in LB medium supplemented with 50 µg/mL kanamycin. Protein expression was induced with 500 µM IPTG and cells were grown at 18 °C overnight. The cells were harvested and stored at -80 °C. Cell pellets were thawed on ice and resuspended in buffer A (500 mM NaCl, 20 mM Tris pH 7.4) supplemented with a complete protease inhibitor tablet (Roche) and 5 mM β-mercaptoethanol (β-ME). The cell suspension was lysed by a microfluidizer (Microfluidics M-110P) at 20000 psi, and was clarified by centrifugation at 30000g for 30 minutes. All purification steps were performed at 4 °C. The clarified lysate was loaded onto a 5 mL HisTrap HP column (GE Healthcare) pre-equilibrated in buffer A. The protein was eluted with buffer A containing 500 mM imidazole. The fractions containing protein were pooled and desalted using a HiPrep 26/10 desalting column (GE Healthcare) equilibrated in buffer A. The desalted protein was then digested with TEV protease at 4 °C and incubated overnight to remove the N-terminal affinity tag. The proteins were passed over a 5 mL HisTrap HP column equilibrated with buffer A, and flow-through containing tag-less protein was collected. The flow-through was further diluted and loaded onto a 5 mL HiTrap Q HP column (GE Healthcare) equilibrated with buffer B (50 mM NaCl and 20 mM Tris pH 8), and eluted with a linear gradient from 0-1000 mM NaCl over 5 column volumes. The eluted protein was concentrated and subjected to size exclusion chromatography using a Highload 16/600 Superdex 75 pg column (GE Healthcare) equilibrated in buffer C (150 mM sodium chloride, 5 mM β-ME, 20% glycerol, and 20 mM Tris pH 7.4). Peak fractions containing protein were pooled, concentrated using a centrifugal concentrator (Millipore, 10K molecular weight cutoff (MWCO)), flash-frozen using liquid nitrogen, and stored at −80 °C.

The SOS^{cat} (human SOS1, residues 558-1049, Uniprot Q07889) plasmid for expression in *E. coli* was a kind gift from Prof. John Kuriyan (University of California, Berkeley). SOS^{cat} was expressed and purified as previously described.(2) In detail, the expression construct includes an N-terminal TEV protease cleavable His_6 tag was transformed into Rosetta 2 DE3 cells (Novagen) and grown in LB medium supplemented with 100 µg/mL ampicillin and 34 µg/mL chloramphenicol. The expression and purification of SOS^{cat} was carried out in a similar fashion as KRas. All mutations were generated using the Q5 site-directed mutagenesis kit (New England Biolabs) following the manufacturer's protocol.

The KRas.SOS^{cat} complex was formed by incubation of the two proteins with three-fold molar excess of KRas-GTP in the presence of 2 mM EDTA at 4 °C overnight. The complex was loaded

into a Highload 16/600 Superdex 75 pg column equilibrated with buffer C. The fractions containing the KRas•SOS^{cat} complex were pooled and concentrated and analyzed using Synapt G1 mass spectrometry under native conditions.

Loading of KRas and mutants with nucleotides. KRas and three oncogenic mutants studied here (G13D, Q61H and G12C) were loaded with either GTP or GDP to monitor the assembly with SOS^{cat}. The nucleotide exchange assay was carried out as described elsewhere.(1) In brief, KRas and oncogenic mutants were incubated with 30 molar excess ratio of either GDP or GTP in the presence of 10 mM EDTA for 3 hours at 4 °C. The reaction mixture was then supplemented with 10 mM $MgCl_2$ and incubated for 30 minutes at 4 °C. Excess nucleotide, $MgCl_2$ and EDTA were removed using a Micro Bio-Spin 6 desalting column (Bio-Rad). The procedure of nucleotide exchange was repeated until full exchange of GDP or GTP was complete as determined by native MS measurements.

Nucleotide exchange assay. To monitor the nucleotide exchange rate, KRas was loaded with B-GDP as explained above, and the excess of B-GDP was removed by HiTrap HP desalting column (GE Healthcare). SOS^{cat} (1 µM) was mixed with KRas-B-GDP (1 µM) at 1:1 molar ratio and incubated in ice for 10 minutes. The SOS^{cat}-mediated nucleotide exchange was initiated by addition of excess 200 µM unlabeled GTP. In order to study the effect of allosteric KRas on nucleotide exchange rate, $KRas^{G13D}$-GTP, $KRas^{WT}$-GTP and $KRas^{Q61H}$-GTP were mixed separately with 200 µM GTP and added to the mixture of SOS^{cat} and KRas-B-GDP and fluorescence (excitation 466.5 nm and emission 512-520 nm) was measured. The final reaction contains 0.5 µM SOS^{cat}, 0.5 µM KRas-B-GDP, 200 µM GTP and 1.5 µM of allosteric KRas-GTP, $KRas^{G13D}$-GTP or $KRas^{Q61H}$-GTP. The nucleotide exchange rate was monitored by a change in fluorescence over time using a Clariostar (BMG labtech) plate reader. The qualitative rate constants were obtained by fitting the data to a single exponential equation.

Inhibitor binding assay. Inhibitors were purchased from Tocris Bioscience (Kobe0065, cat no:5475, BAY-293, cat no:6857), Chemietek (ARS1620, cat no: CT-ARS1620) and TargetMol (BI-3406, cat no: T12979). To confirm the specificity of ARS-1620 for inactive state of $KRas^{G12C}$, 10 µM ARS-1620 was mixed with 3 µM $KRas^{G12C}$-GDP or $KRas^{G12C}$-GTP and native mass spectra was collected (Fig. S8). In order to study the ability of ARS-1620 to disrupt the $KRas^{G12C}$ complexed with SOS^{cat}, 10 µM ARS-1620 was added to pre-incubated complex (1 µM SOS^{cat} mixed with 3 µM $KRas^{G12C}$-GDP or $KRas^{G12C}$-GTP incubated for five minutes) and the mixture was incubated for another 60 minutes in ice and native mass spectra were recorded. Similar experiments were carried out to test the ability of BAY-293 and Kobe0065 to disrupt binary and ternary complexes of SOS^{cat} and KRas, $KRas^{G13D}$ and $KRas^{G12C}$. 2.5 µM BAY-293 was added to pre-incubated mixtures of 1 µM SOS^{cat} and 3 µM of KRas-GTP or $KRAS^{G13D}$-GTP and incubated in ice for 60 minutes and subsequent native mass spectrum was recorded. Similar experiments were performed with BAY-

293 on SOS^{W729E} complexes with KRas-GDP and $KRas^{G13D}$-GDP. Mass spectra of 2.5 µM Kobe0065 added to pre-incubated mixtures of 1 µM SOS^{cat} and 3 µM KRas-GTP or $KRas^{G13D}$-GTP were also recorded.

Inorganic phosphate assay. The phosphate concentration of KRas alone and in the presence of SOS^{cat} was measured using a malachite green assay.(3) In brief, malachite green reagent (1 mg/mL malachite green, 100 mg/ mL ammonium molybdate, and 0.01% Triton X-100 in 50 mL of 1 M hydrochloric acid) was prepared as described previously.(4) KRas-GTP was mixed with SOS^{cat} and incubated for 5 minutes on ice. To determine the phosphate concentrations of complex mixture and control solutions (KRas-GTP and SOS^{cat} alone), 40 µl malachite green reagent was added individually to 10 µl of control solution or complex mixture and incubated for 15 minutes at room temperature. Absorbance was measured at 650 nm using a Clariostar (BMG labtech) plate reader and subtracted from buffer. A standard curve was generated by serial dilutions of 1 mM dipotassium phosphate. All measurements were done in triplicate, and solutions were made using OmniTrace Ultra water (Sigma-Aldrich) to minimize background phosphate.

Native Ion mobility mass spectrometry. The solution dynamics and conformational heterogeneity of SOS^{cat} in the presence and absence of KRas was analyzed using an Agilent 6560 ion mobility Q-TOF mass spectrometer (Agilent Technologies, Santa Clara, CA). A home-built nano-electrospray ionization source was used to generate native-like ions to preserve non-covalent interactions and pulsed into the drift tube filled with nitrogen gas for ion mobility measurements. To determine the first-principle CCS calculations,(5) the arrival time distributions were plotted as a function of drift voltage to determine the time ions spend outside the drift tube. CCS was calculated using the Mason-Schamp equation(6) with the following instrumental parameters: pressure (~3.915 torr), temperature (24.5 °C) and drift length (78 cm). Instrumental settings are provided in Table S5 and S6.

Collision-induced and Surface-induced dissociation experiments. Collision-induced dissociation experiments were performed on Synapt G1 (Waters). The ternary complexes of KRas or $KRas^{G12C}$ with SOS^{cat} were mass isolated in the quadrupole and activated inside the trap region. The instrument parameters were set to a capillary voltage 1.8 kV, sampling cone 50 V, extraction cone 5 V, low mass resolution 3.5, trap collision energy 100 V, transfer collision energy 10 V, Trap gas flow 2 ml/min and source temperature of 90 °C. For SID experiments, samples were analyzed using Synapt G2 (Waters) tuned to maximize signal while preserving non-covalent interactions. Some parameters include capillary voltage 1.2 kV, sampling cone 20 V, extraction cone 1 V, trap gas flow 4 ml/min, He flow 120 ml/min, IMS (N_2) flow 60 ml/min and source temperature of 30 °C. For mass selection of all charge states of ternary complex, the quad profile was set to manual range = 6000 m/z. SID design and surface modification has been previously described (7).

Data collection for single-particle cryo-EM. The $KRas^{G13D}$•SOS^{cat}•$KRas^{G13D}$-GppNp complex was concentrated to 8.6 mg/mL for cryo-EM grid preparation. To reduce protein aggregation, 0.5% fluorinated octyl maltoside (Anatrace) was added to the samples to a final concentration of 0.05% prior to freezing. Sample vitrification was performed using a Vitrobot Mark IV (Thermo Fisher) operating at 8 ^{o}C and 100% humidity. A total of 3.5 µL of the sample was applied to holey carbon grids (Quantifoil 200 mesh Cu 1.2/1.3) glow-discharged for 30 seconds. The grids were blotted for 1 second at a blotting force of 1 using standard Vitrobot filter paper (Ted Pella, 47000-100), and then plunged into liquid ethane.

Frozen grids were shipped to the National Center for Cryo-EM Access and Training (NCCAT) for data collection. The dataset was acquired as movie stacks with a Titan Krios electron microscope operating at 300 kV, equipped with a K3 direct detector camera. Images were recorded at a magnification of 105,000x at super-resolution counting mode by image shift. The total exposure time was set to 2.5 s with a frame recorded every 0.05 s, resulting in 50 frames in a single stack with a total exposure around 65 electrons/$Å^2$. The defocus range was set at -0.8 to -2.5 µm. See Table S7 for the details.

Image Processing. Stack images were subjected to beam-induced motion correction by MotionCor2.(8) CTF parameters for each micrograph were determined by CTFFIND4.(9) The following particle selection, two- and three-dimensional classifications, three-dimensional refinement, and post-processing were performed in RELION-3.1.(10) The detailed data processing flow is shown in Fig. S11. Briefly, particles were selected by automatic picking, using the 2D templates generated from ~2,000 manually picked particles. Contamination and poorly-aligned classes were disposed after 2D classification. 2,294,620 particles were selected for the initial 3D classification using a previously reported HRas•SOS^{cat}•HRas-GDP complex (PDB 1XD2) as a reference model, followed by 3D refinement, post-processing, CTF refinement, and Bayesian polishing performed on the best class. The final map for the $KRas^{G13D}$•SOS complex was resolved at 3.47 Å.

Model Building, Refinement, and Validation. Previously reported HRas•SOS^{cat}•HRas-GDP complex structure (PDB 1XD2) was docked into the cryo-EM map as a rigid body using Chimera (11). HRas-GTP bound at the allosteric site was replaced by aligning the $KRas^{G13D}$ bound to GppNp (PDB 6E6F) in Coot (12). In a similar fashion, the HRas molecule bound at the active site was replaced by aligning $KRas^{G12C}$ (PDB 6EPL) followed by mutation of residues to match the $KRas^{G13D}$ sequence in Coot. After these operations, the model was manually refined using Coot(12) followed by one round of real-space refinement using Phenix(13) with secondary-structure and Ramachandran restraints. Geometry outliers were manually fixed in Coot. The statistics of the final round of model refinement and the model geometry are shown in Table S8.

Supporting Figures

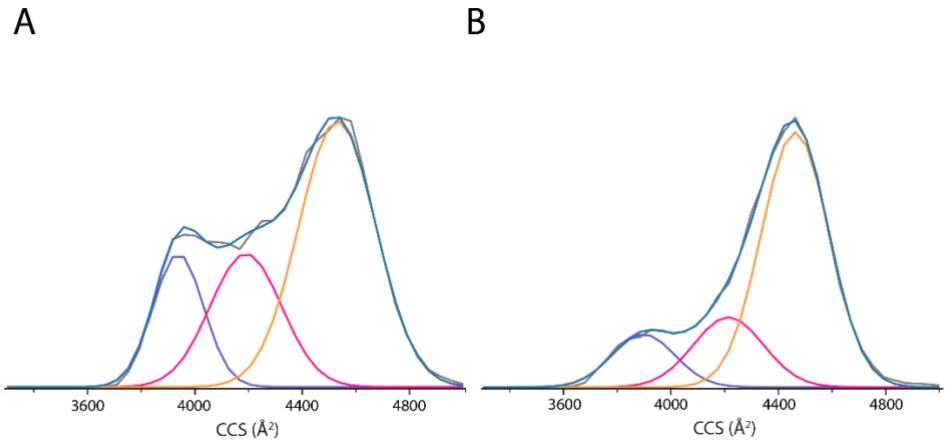

Figure S1. Conformational dynamics of SOS^{cat} captured by ion mobility spectrometry. Collision cross section plots (blue lines) of SOS^{cat} for 17^{+} charge state in the (A) absence and (B) presence of KRas. Regression (R^2 = 1.0) of three Gaussian peaks (purple, pink and orange lines) and their sum (grey lines).

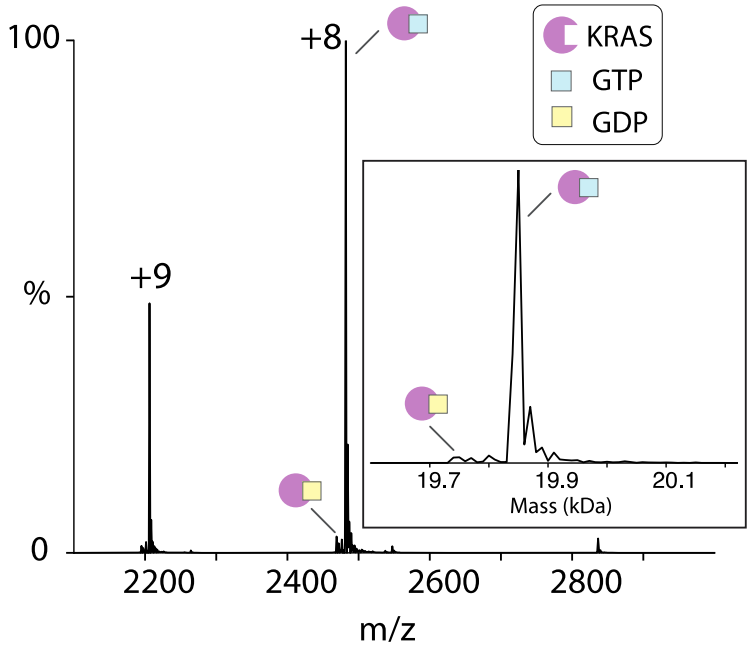

Figure S2. The low *m/z* region of the mass spectrum of KRas-GTP complexed with SOS^{cat}. Deconvolution of the mass spectrum shows KRas is predominantly loaded with GTP.

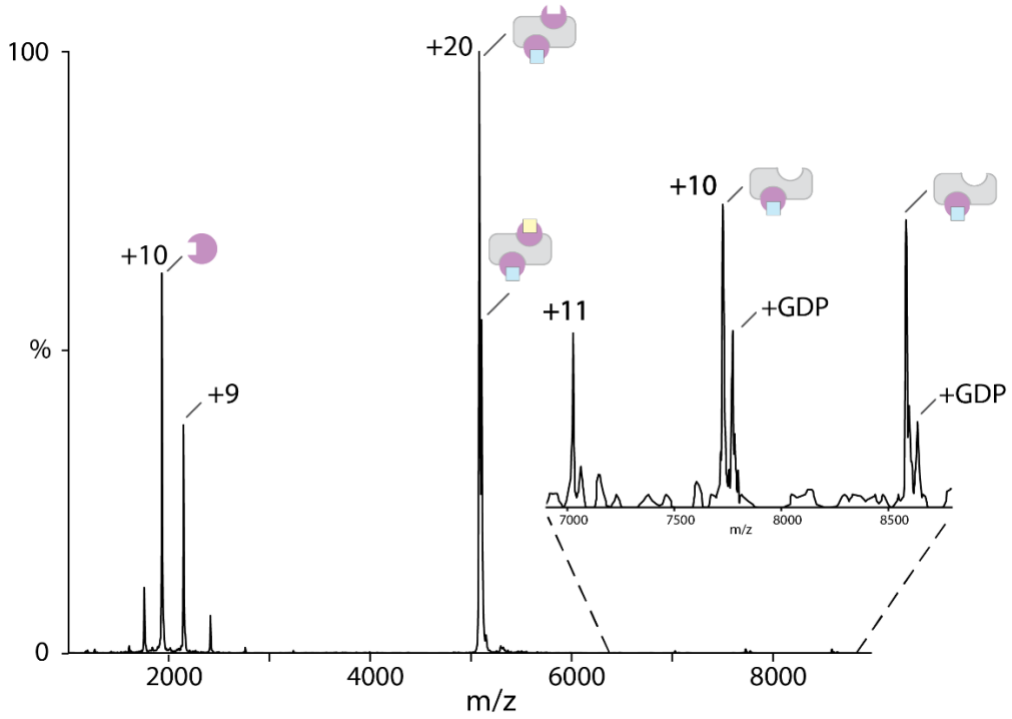

Figure S3. Mass spectrum of the ternary KRas•SOS^{cat} •KRas-GTP.Mg^{2+}(GDP)$_1$ complex post collisional activation. The 20$^+$ charge state of ternary complex was isolated and subsequently activated in the collision cell. The peaks at low *m/z* range correspond to KRas apo and those in higher *m/z* range represent SOS^{cat}•KRas-GTP-Mg^{2+} with a peak corresponding to bound GDP.

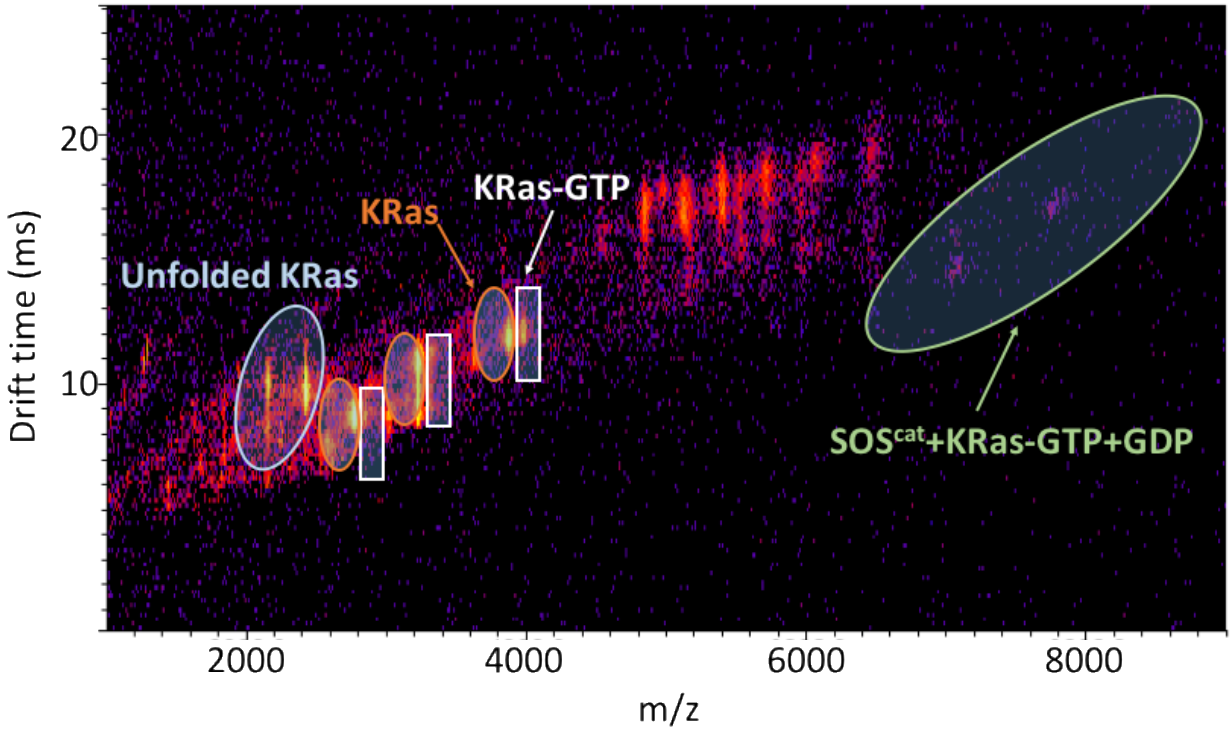

Figure S4. Surface induced dissociation of the KRas•SOS^{cat} •KRas-GTP.Mg^{2+}(GDP) complex. The charge state distribution of ternary complex was selected in quadruple prior to surface induced dissociation. The dissociated species are labeled.

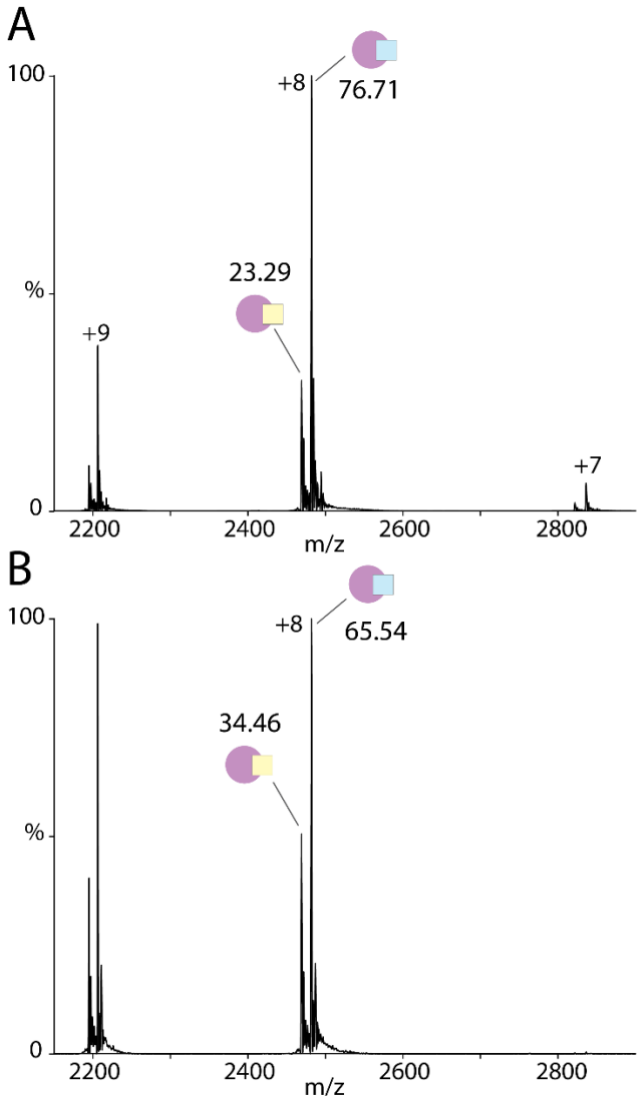

Figure S5. Native mass spectra of (A) KRas-GTP and (B) KRas-GTP in the presence of SOS^{cat} incubated at 4 °C for 22 hours. The mole fractions of KRas bound GDP and GTP were determined after deconvoluting the mass spectra using Unidec.(14) The low *m/z* range mass spectra show higher abundance of K-Ras bound GDP for KRas-GTP complexed with SOS^{cat} compared to KRas-GTP alone shown in A.

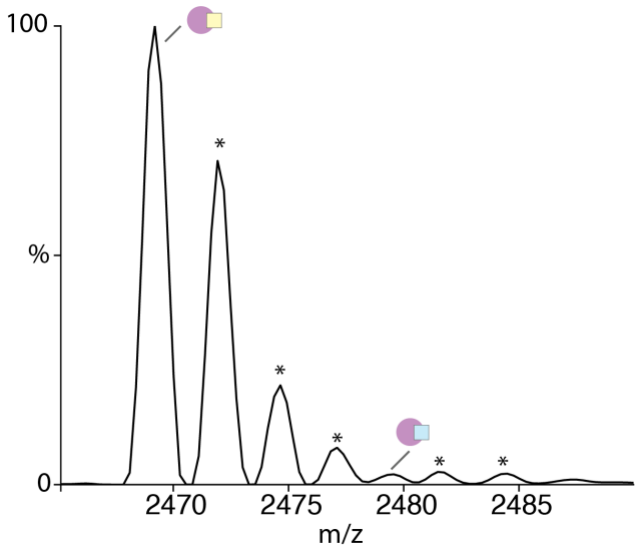

Figure S6. KRas loaded with GDP shows the presence of a negligible fraction of GTP. Shown is a zoom of the 8^+ charge state with magnesium or sodium bound adducts denoted by an asterisk.

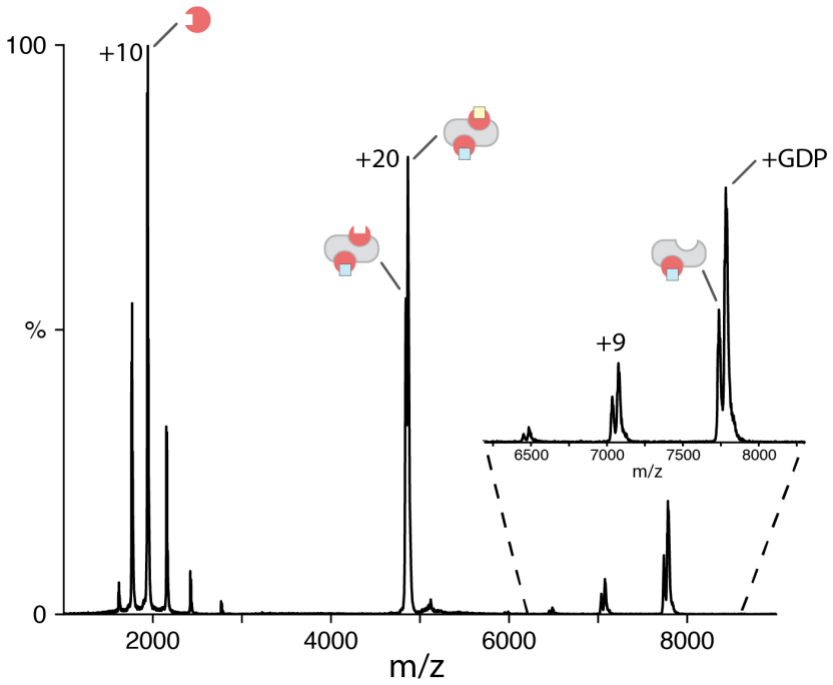

Figure S7. The representative mass spectrum for collisional activation of the ternary $KRas^{G12C}$•SOS^{cat}•$KRas^{G12C}$-GTP-$Mg^{2+}(GDP)_1$ complex. The 20^+ charge state of complex was isolated and subsequently activated in the collision cell. The peaks at low *m/z* range correspond to apo K-Ras^{G12C} and those in higher *m/z* range represent SOS^{cat}•K-Ras^{G12C}-GTP.Mg^{2+} with a peak corresponding to bound GDP.

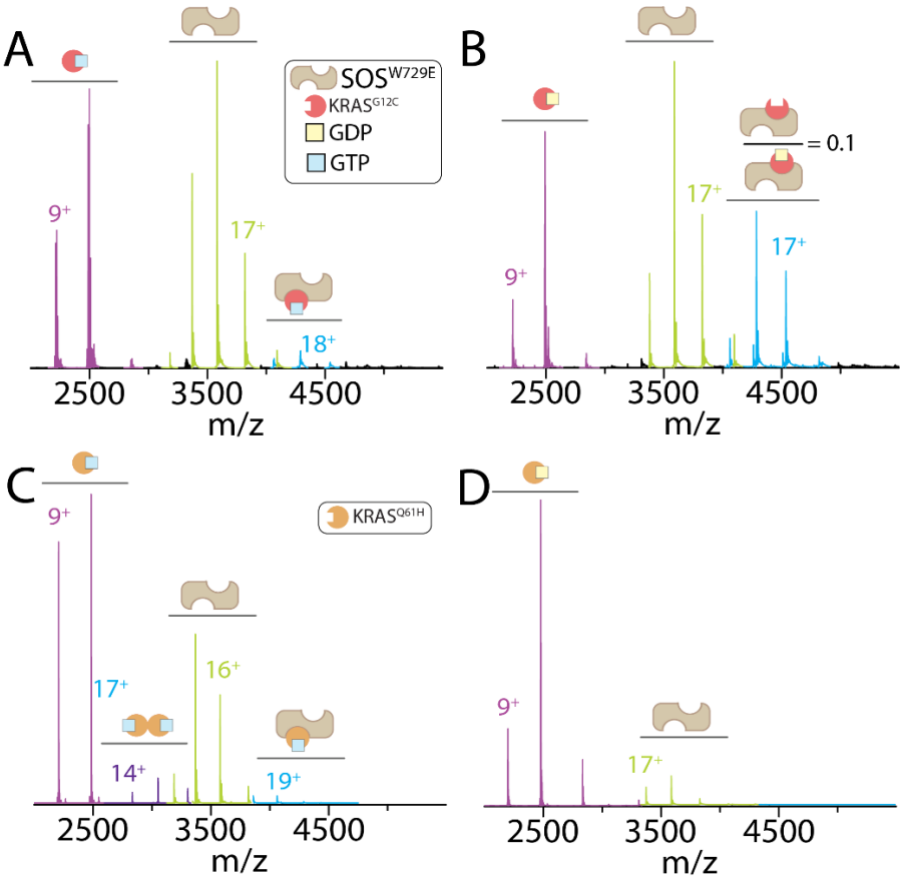

Figure S8. Complexes of SOS^{cat} mutant with KRas and oncogenic mutants. (A-D) Native mass spectra of 2 µM SOS^{W729E} mixed with 6 µM of (A) KRas^{G12C}-GTP, (B) KRas^{G12C}-GDP, (C) KRas^{Q61H}-GTP and (D) KRas^{Q61H}-GDP.

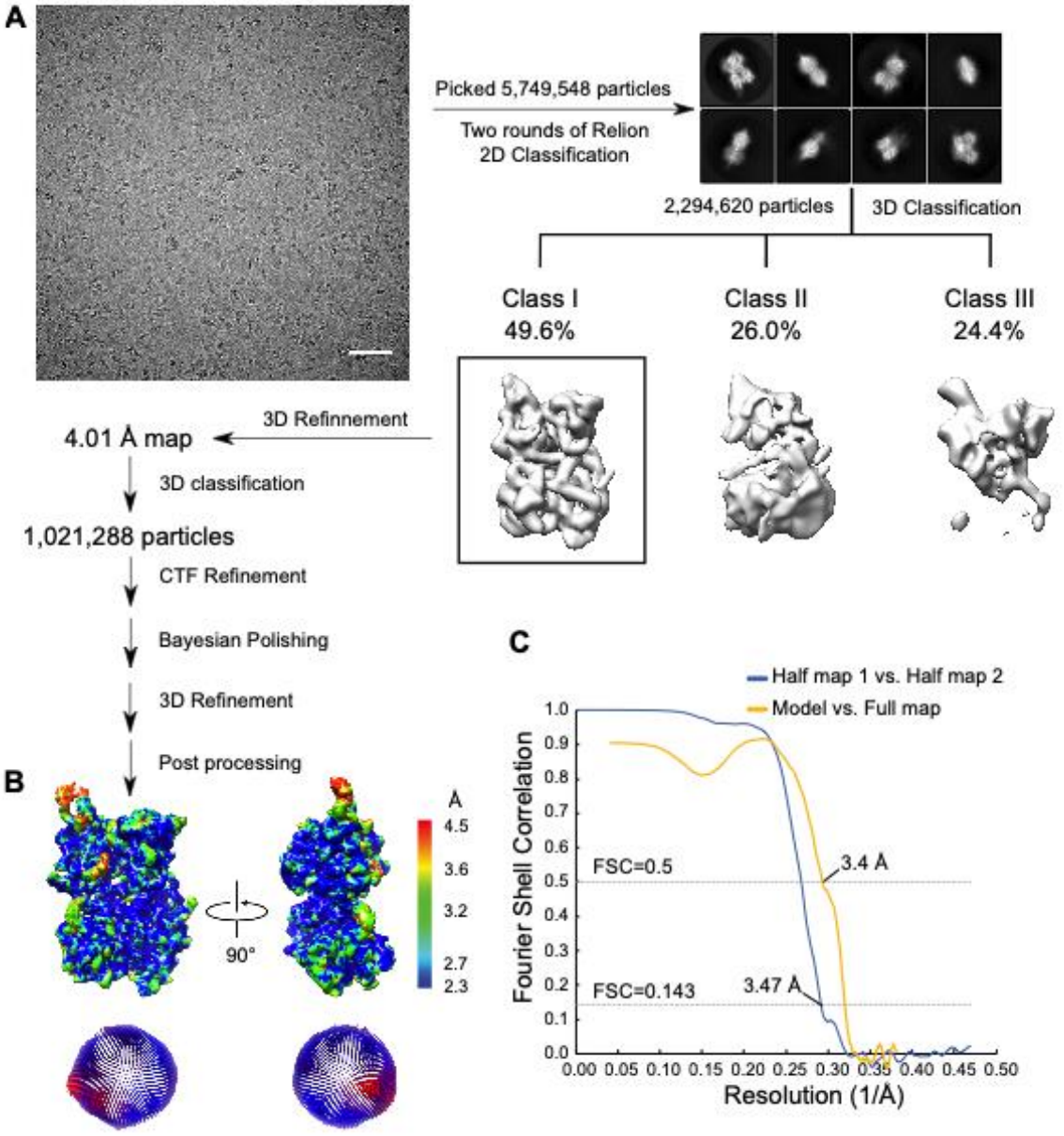

Figure S9. Single-particle cryo-EM analysis for the KRas^{G13D}•SOS^{cat} complex. (A) The workflow of data processing. The data was acquired at the National Center for CryoEM Access and Training (NCCAT) using a Titan Krios electron microscope operating at 300 KV. Initial motion correction was carried out using MotionCor2.(8) A representative micrograph is shown along with a scale bar corresponding to 50 nm. The following steps were performed in Relion.(10) Representative 2D class averages are shown, with the box edge corresponding to 170 Å. After disposing contamination and poorly-aligned 2D classes, three maps were resolved using 3D classification. Subsequent refinement and polishing were performed on the best 3D class. (B-C) Fourier shell correlation curves of the half map 1 versus the half map 2 (blue), and the refined model versus the overall map (yellow). The resolution of the reconstruction was determined by the FSC=0.143 criterion.

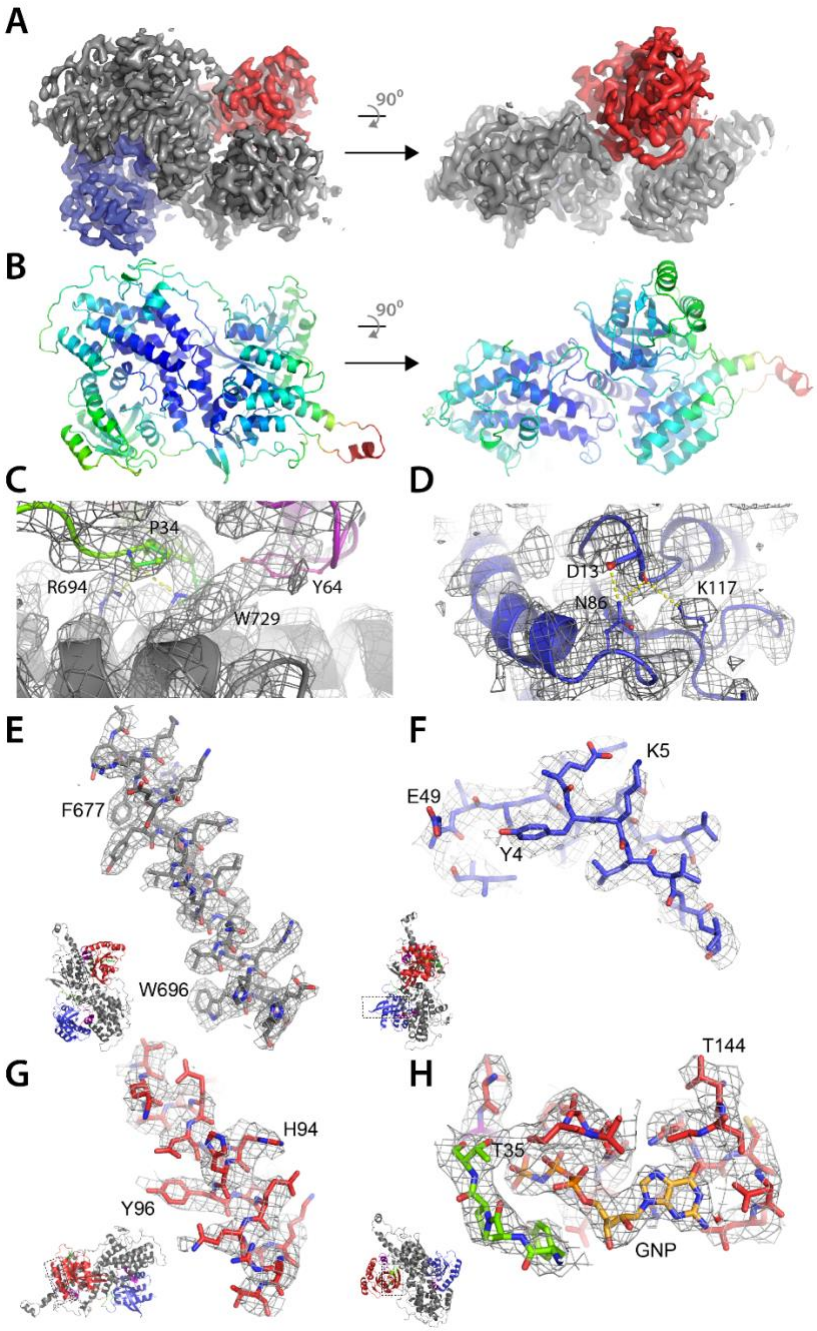

Figure S10. Atomic model of the ternary KRas^{G13D}•SOS^{cat} complex and the cryoEM density. (A) The cryoEM density map of the overall structure contoured at 6 rmsd. Density corresponding to KRas^{G13D} molecules bound at the active and allosteric sites of SOS^{cat} (grey) are colored blue and red, respectively. (B) The structure shown in cartoon representation and color-coded by B-factor, ranging from 22 (dark blue) to 142 (red) Å^2. Selected regions along with density map are shown: (C-D) KRas^{G13D} molecules bound at the allosteric and active sites of SOS^{cat}, respectively; (E) an α-helix of SOS^{cat}, contour level 5.0 rmsd; (F) a β-sheet of K-Ras^{G13D} at the active site, contour level 5.0 rmsd; (G) an α-helix of KRas^{G13D} at the allosteric site, contour level 5.0 rmsd; and (E) GppNp (GNP) of KRas^{G13D} at the allosteric site, contour level 6.0 rmsd.

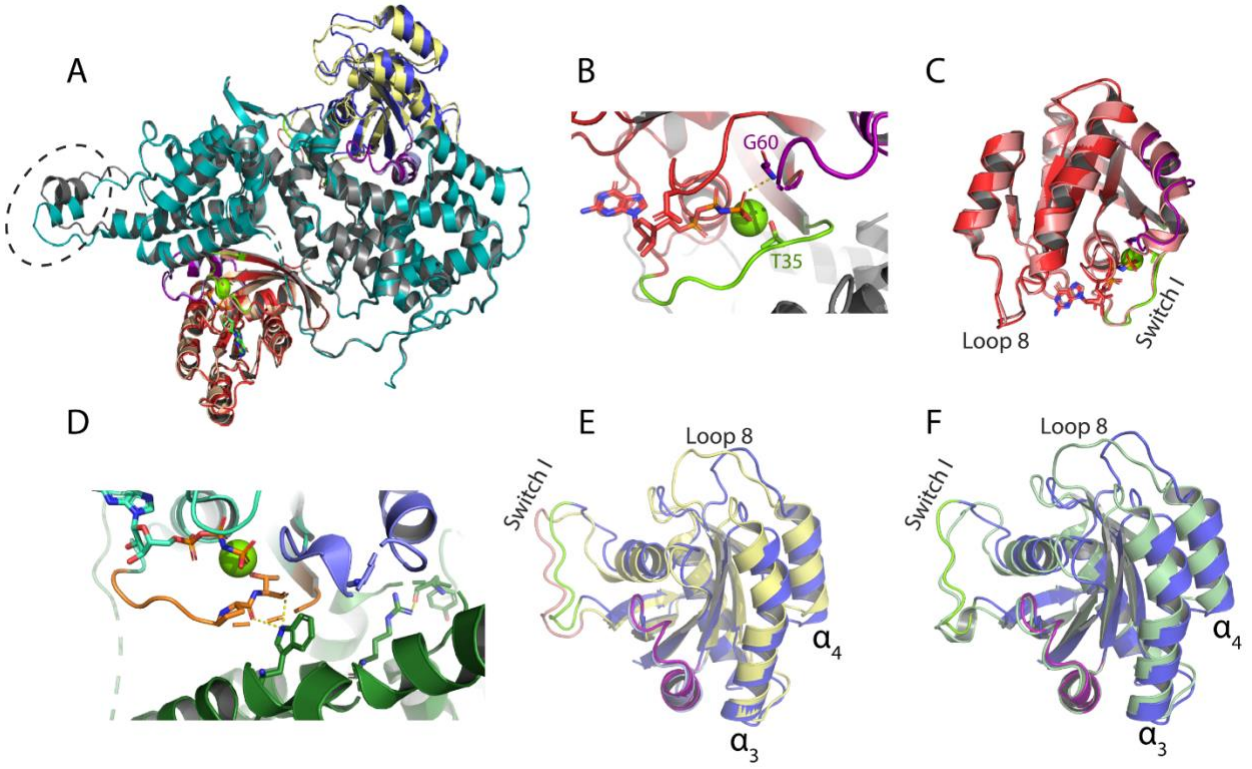

Figure S11. Comparison of the structure of KRas^{G13D} in complex with SOS^{cat} to other structures. (A) Superimposition of the KRas^{G13D} ternary structure with the crystal structure of H-Ras-GppNp in complex with SOS^{cat} (PDB id: 1NVW) yielding an RMSD of 2.5 Å. The KRas^{G13D} is shown as in figure 4. For the HRas complex, SOS^{cat} is colored cyan (SOS^{cat}), the active site yellow, and allosteric site wheat. A notable shift in the α3 and α4 helices by ~2.5 Å. (B) The interaction of Thr35 and Gly60 residues with the phosphate of GppNp bound to KRas^{G13D}. (C) Alignment of KRas^{G13D}-GTP with HRas-GppNp (PDB 3K8Y). (D) Molecular interactions of HRas-GppNp (PDB id: 1NVV) at the allosteric site of SOS^{cat}. (E-F) Superimposition of K-Ras^{G13D} bound at the active site with (E) HRas and (F) KRas^{G12C} (PDB 6EPP).

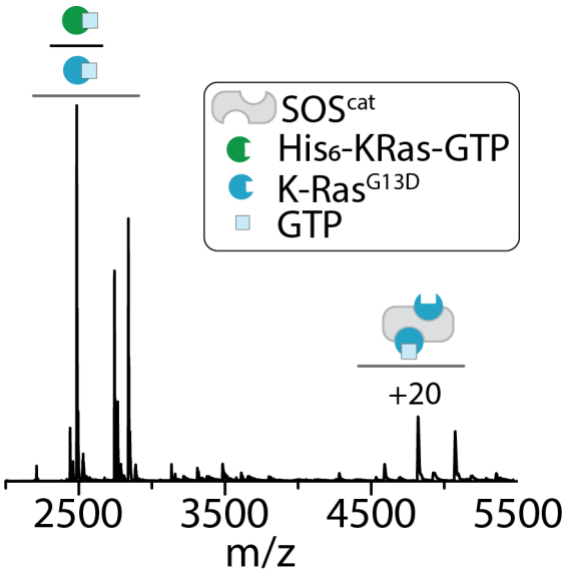

Figure S12. KRas does not dissociate KRas^{G13D} bound at either the allosteric and active site of SOS^{cat}. The addition of His_6-KRas (3 µM final concentration) to pre-incubated mixture of 1 µM SOS^{cat} and 3 µM KRas^{G13D}-GTP.

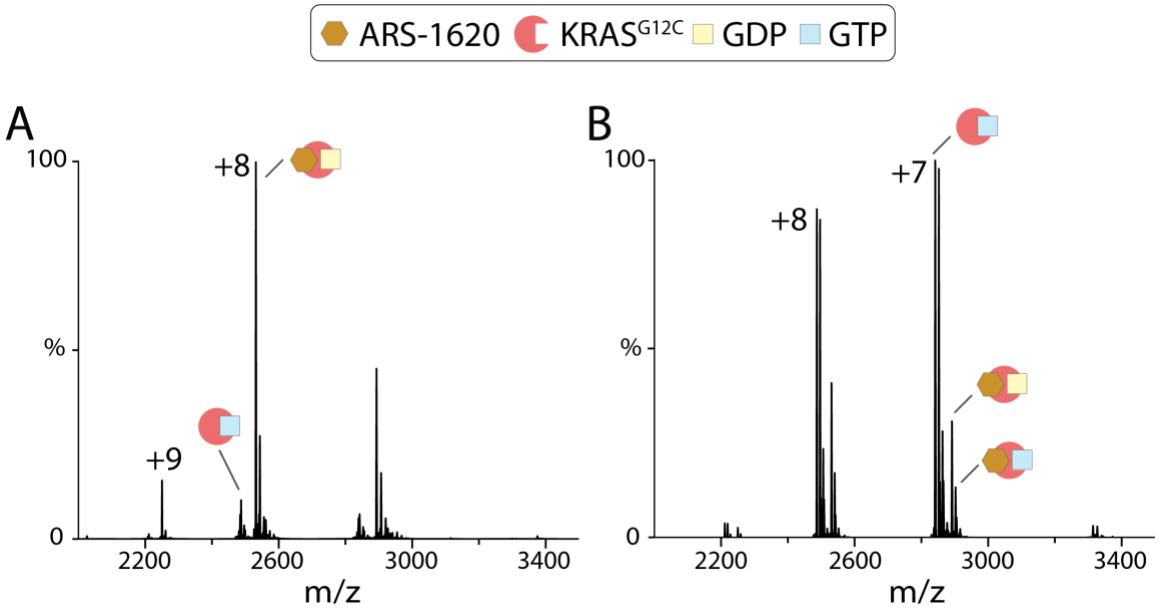

Figure S13. The specificity of ARS-1620 towards the inactive state of KRas^{G12C}. The native mass spectra recorded for 10 µM ARS-1620 mixed with 3 µM (A) KRas^{G12C}-GDP or (B) KRas^{G12C}-GTP.

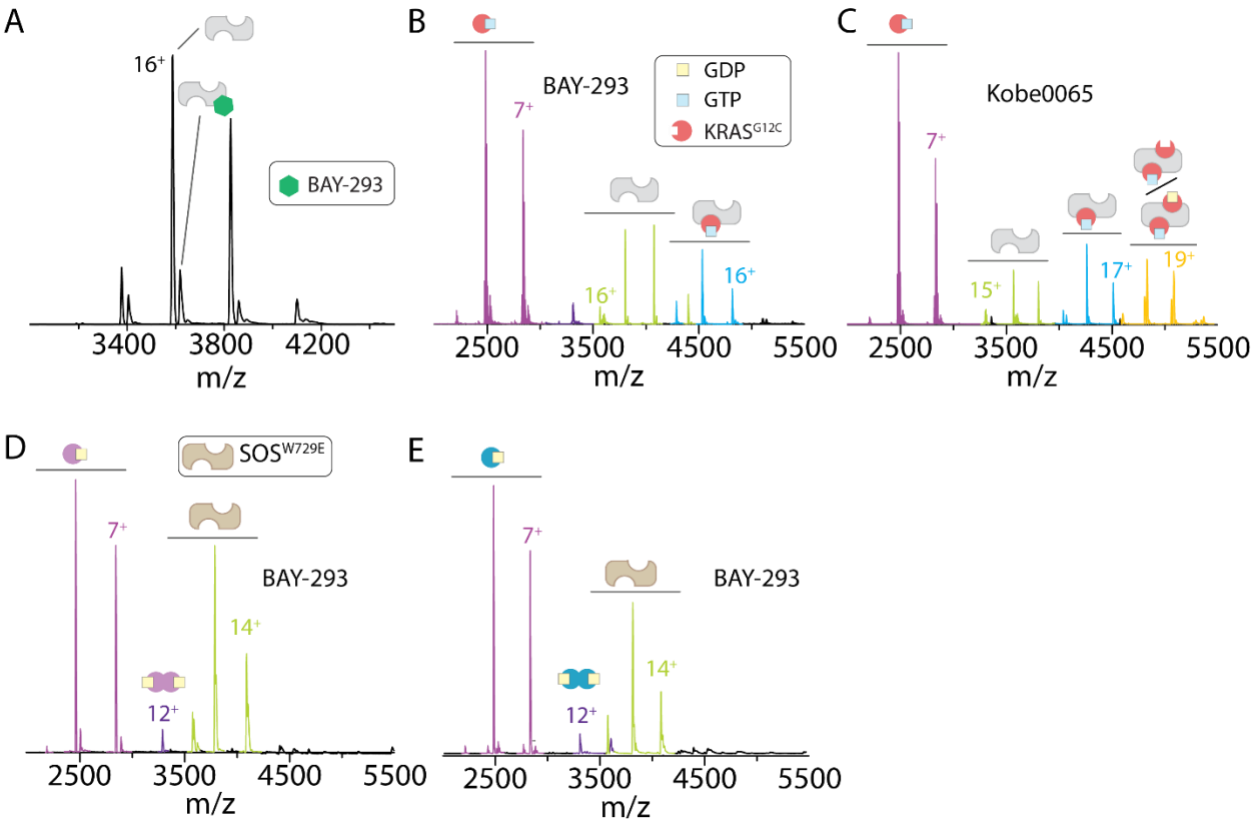

Figure S14. Kobe0065 does not disrupt the complexes of SOS^{cat} with KRas^{G12C}. (A) Native mass spectrum of 2 µM SOS^{cat} and 10 µM of BAY-293. (B-C) The addition of (B) BAY-293 or (C) Kobe0065 at final concentration of 2.5 µM to a pre-incubated mixtures of 1 µM SOS^{cat} and 3 µM KRas^{G12C}-GTP. The addition of 2.5 µM BAY-293 to a pre-incubated mixtures of 1 µM SOS^{W729E} with 3 µM of (D) KRas-GTP or (E) KRas^{G13D}-GDP.

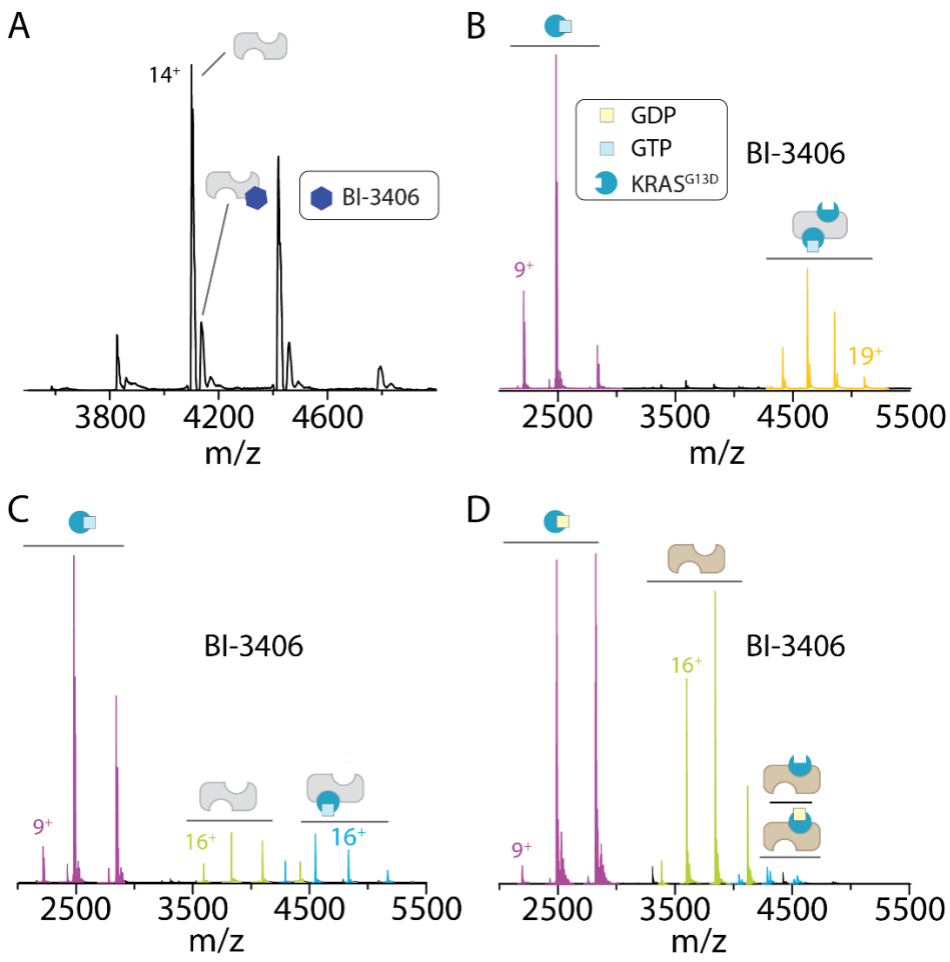

Figure S15. BI-3406 interaction with SOS^{cat} and SOS^{W729E}:KRas^{G13D}-GDP and SOS^{cat}:KRas^{G13D}-GTP complexes. (A) Native mass spectrum of 1 µM SOS^{cat} and 5 µM of BI-3406. (B-C) The mass spectra of (B) 2.5 µM and (C) 20 µM BI-3406 added to a complex of 1 µM SOS^{cat} and 3 µM KRas^{G13D}-GTP and incubated overnight at 4 °C. (D) Addition of 2.5 µM BI-3406 to a pre-incubated mixture of 1 µM SOS^{W729E} and 3 µM KRas^{G13D}-GDP.

Supporting tables

Table S1. CCS values for different conformers of SOS^{cat} determined from first-principle measurements. Reported are the mean and standard deviation (*n* = 3).

Conformer	CCS (Å, $z = 16^+$)	CCS (Å, $z = 17^+$)
1	3840 ± 20	3915 ± 22
2	4095± 21	4195 ± 5
3	4378 ± 2	4464 ± 10

Table S2. Theoretical and measured masses for molecular assemblies of SOS^{cat} and KRas and oncogenic mutants. The asterisk denotes Na^+ or Mg^{2+} adducts.

Detected ion	*Measured mass (Da)*	*Theoretical mass (Da)*	*Δ Da*
SOS^{cat}	57366.20	57369.84	3.64
SOS^{W729E}	57316.24	57312.74	3.50
$KRas^{WT}$-GDP	19746.48	19746.00	0.48
$KRas^{WT}$-GTP	19828.96	19825.98	2.98
SOS^{cat}•KRas-GTP-Mg^{2+}	77222.31	77218.82	3.49
KRas•SOS^{cat}•KRas-GTP-Mg^{2+}	96530.23	96521.62	8.61
KRas•SOS^{cat}•KRas-GTP-Mg^{2+}-$H_2PO_4^-$	96612.12	96618.61	6.49
KRas•SOS^{cat}•KRas-GTP-$Mg^{2+}$$(GDP)_1$	96972.20	96964.82	7.38
KRas•SOS^{cat}•KRas-GTP-Mg^{2+}-$H_2PO_4^-$$(GDP)_1$	97060.15	97061.81	1.66
KRas•SOS^{cat}	76673.41	76672.64	0.77
KRas-GDP•SOS^{cat}	77117.63	77115.84	1.79
KRas•SOS^{W729E}	76622.94	76615.54	7.40
KRas-GDP•SOS^{W729E}	77064.33	77058.74	5.59
KRas•SOS^{W729E}•KRas-GTP-Mg^{2+}	96474.60	96464.52	10.08
KRas•SOS^{W729E}•KRas-GTP-$Mg^{2+}$$(GDP)_1$	96915.22	96907.72	7.50
SOS^{cat}•KRas-B-GTP-Mg^{2+}	77582.43	77578.19	4.24
KRas•SOS^{cat}•KRas-GTP. $Mg^{2+}$$(B\text{-}GDP)_1$	97332.87	97324.00	8.87
KRas•SOS^{cat}•KRas-GTP-Mg^{2+}-$H_2PO_4^-$$(B\text{-}GDP)_1$	97413.92	97420.99	7.07
KRas•SOS^{cat}•KRas-B-GTP. $Mg^{2+}$$(B\text{-}GDP)_1$	97693.44	97683.37	10.07
$KRas^{G13D}$•SOS^{cat}•$KRas^{G13D}$-GTP-Mg^{2+}	96641.72	96639.84	1.88
$KRas^{G13D}$•SOS^{cat}	76731.74	76731.84	0.10
$KRas^{G13D}$•$SOS^{cat}$$(GDP)_1$	77179.58	77174.84	4.74
$KRas^{G13D}$•SOS^{cat}•$KRas^{G13D}$-GDP*	96555.17	96536.84	18.33
$KRas^{G13D}$•SOS^{cat}•$KRas^{G13D}$-GDP$(GDP)_1$*	96999.91	96979.84	20.07
$KRas^{G13D}$•SOS^{W729E}	76674.91	76674.74	0.17
$KRas^{G13D}$•SOS^{W729E}•$KRas^{G13D}$-GTP-Mg^{2+}	96589.25	96582.74	6.51
$KRas^{G13D}$•SOS^{W729E}	76671.86	76674.74	2.88
$KRas^{G13D}$•$SOS^{W729E}$$(GDP)_1$	77117.28	77117.74	0.46
SOS^{cat}•$KRas^{G12C}$-GTP-Mg^{2+}	77268.65	77263.84	4.81
$KRas^{G12C}$•SOS^{cat}•$KRas^{G12C}$-GTP-Mg^{2+}	96612.72	96611.84	0.88
$KRas^{G12C}$•SOS^{cat}•$KRas^{G12C}$-GTP-$Mg^{2+}$$(GDP)_1$	97056.77	97054.84	1.93
$KRas^{G12C}$•SOS^{cat}	76721.45	76717.84	3.61
$KRas^{G12C}$-GDP•SOS^{cat}	77167.11	77160.84	6.27
$KRas^{G12C}$•SOS^{W729E}	76664.43	76660.74	3.69
$KRas^{G12C}$-GDP•SOS^{W729E}	77111.28	77103.74	7.54
SOS^{W729E}•$KRas^{G12C}$-GTP-Mg^{2+}	77205.00	77206.74	1.74
SOS^{cat}• $KRas^{Q61H}$-GTP-Mg^{2+}	77225.82	77228.83	3.01
$KRas^{Q61H}$-GDP•SOS^{cat}	77134.22	77125.83	8.39
SOS^{W729E}•$KRas^{Q61H}$-GTP- Mg^{2+}	77178.71	77171.73	6.98

Table S3. Inorganic phosphate (P_i) concentrations measured by malachite green assay for KRas-GTP, SOS^{cat} and KRas-GTP in complex with SOS^{cat}. Reported are the mean and standard deviation (*n* = 3).

	$[P_i]$ (μM)	
Complex	37.64 ± 0.79	-
KRas-GTP	16.05 ± 0.87	-
SOS^{cat}	7.36 ± 0.28	-
$[P_i]'_{complex} = [P_i]_{complex} - [P_i]_{SOS^{cat}}$	30.28 ± 0.84	-
$[P_i]'_{complex}/[P_i]_{KRas\text{-}GTP}$	-	1.88 ± 0.11

Table S4. Tuned instrument parameters used for monitoring the assembly of KRas and mutants with SOS^{cat} or SOS^{W729E} using an orbitrap mass spectrometer.

Instrument Parameters	
m/z range	1000-8000
Resolution	8000
In-source collision energy dissociation (V)	100
Collision energy	10
Source temperature (°C)	100
Capillary voltage (KV)	1.5
Source DC offset (V)	25
Injection flatapole lens(V)	18
Inter flatapole DC (V)	4
Bent flatapole DC (V)	5
Transfer multipole DC (V)	2
Pressure (mbar)	3×10^{-10}

Table S5. Instrument tuning parameters for settings for Agilent 6560.

Instrument Parameters	
Capillary voltage (V)	1000-2000
Drying gas temperature (℃)	200
Drying gas flow (L/min)	1.5
Fragmentor (V)	400
High Pressure funnel delta (V)	150
High Pressure Funnel RF (V)	200
Trap funnel delta (V)	180
Trap funnel RF (V)	200
Trap Funnel Exit (V)	10

Table S6. Drift Tube Settings for Stepped Field Experiments in Positive Ion Mode on the Agilent 6560.

Sequence	Time (min)	Drift Tube Entrance (V)	Drift Tube Exit (V)	Rear Funnel Entrance (V)	Rear Funnel Exit (V)
1	0.0 – 0.5	1074	224	217.5	45
2	0.5 – 1.0	1174	224	217.5	45
3	1.0 – 1.5	1274	224	217.5	45
4	1.5 – 2.0	1374	224	217.5	45
5	2.0 – 2.5	1474	224	217.5	45
6	2.5 – 3.0	1574	224	217.5	45
7	3.0 – 3.5	1674	224	217.5	45

Table S7. Statistics of cryo-EM data collection and processing

	$KRas^{G13D}$•SOS^{cat}•KRas-GppNp
Microscope	Krios (NCCAT)
Magnification	105,000
Voltage (kV)	300
Spherical aberration (mm)	2.7
Detector	K3
Camera mode	Super resolution counting
Exposure rate (e^-/pixel/s)	30
Total exposure ($e^-/Å^2$)	65
Defocus range (μm)	-0.8 to -2.5
Pixel size (Å)	0.5325 (1.065 physical)
Mode of data collection	Image shift
Energy filter	30 eV slit
Software for data collection	Leginon
Number of micrographs	5,202
Symmetry imposed	C1
Box size (pixel)	192
Initial particle images (no.)	5,749,548
Particle images for 3D (no.)	2,294,620
Final particle images (no.)	1,021,288
Map resolution, unmasked (Å)	3.85
Map resolution, masked (Å)	3.47
B-factor used for sharpening ($Å^2$)	-162
EMD code	EMD-22857
PDB code	7KFZ

Table S8: Statistics of cryo-EM refinement and geometry.

Model	
Composition (#)	
Chains	3
Atoms	6592 (Hydrogens: 0)
Residues	Protein: 803 Nucleotide: 0
Water	0
Ligands	GNP: 1; MG: 1
Bonds (RMSD)	
Length (Å) (# > 4σ)	0.011 (0)
Angles (°) (# > 4σ)	0.739 (0)
MolProbity score	1.74
Clash score	8.98
Ramachandran plot (%)	
Outliers	0.00
Allowed	3.79
Favored	96.21
Rama-Z (Ramachandran plot Z-score, RMSD)	
whole (N = 791)	0.09 (0.26)
helix (N = 66)	0.61 (0.61)
sheet (N = 39)	0.31 (0.74)
loop (N = 686)	0.02 (0.21)
Rotamer outliers (%)	0.00
Cβ outliers (%)	0.00
Peptide plane (%)	
Cis proline/general	2.5/0.0
Twisted proline/general	2.5/0.0
CaBLAM outliers (%)	0.51
ADP (B-factors)	
Iso/Aniso (#)	6592/0
min/max/mean	
Protein	16.71/134.24/45.48
Ligand	34.99/43.46/43.20
Data	
Box	
Lengths (Å)	73.48, 100.11, 124.61
Angles (°)	90.00, 90.00, 90.00
Supplied Resolution (Å)	3.5
Resolution Estimates (Å)	Masked
d FSC (half maps; 0.143)	3.4
d 99 (full/half1/half2)	3.3/4.1/4.1
d model	3.5
d FSC model (0/0.143/0.5)	3.0/3.1/3.4
Map min/max/mean	-0.14/0.24/0.00
Model vs. Data	
CC (mask)	0.86
CC (box)	0.75
CC (peaks)	0.74
CC (volume)	0.84
Mean CC for ligands	0.93

Supplementary References

1. Z. Moghadamchargari *et al.*, Intrinsic GTPase Activity of K-RAS Monitored by Native Mass Spectrometry. *Biochemistry* **58**, 3396-3405 (2019).
2. S. M. Margarit *et al.*, Structural evidence for feedback activation by Ras.GTP of the Ras-specific nucleotide exchange factor SOS. *Cell* **112**, 685-695 (2003).
3. P. A. Lanzetta, L. J. Alvarez, P. S. Reinach, O. A. Candia, An improved assay for nanomole amounts of inorganic phosphate. *Analytical Biochemistry* **100**, 95-97 (1979).
4. A. Quan, P. J. Robinson, "Rapid Purification of Native Dynamin I and Colorimetric GTPase Assay" in Methods in Enzymology. (Academic Press, 2005), vol. 404, pp. 556-569.
5. J. W. McCabe *et al.*, THE IMS PARADOX: A PERSPECTIVE ON STRUCTURAL ION MOBILITY-MASS SPECTROMETRY. *Mass Spectrometry Reviews* **n/a** (2020).
6. E. A. Mason, E. W. McDaniel, Transport properties of ions in gases. *NASA STI/Recon Technical Report A* **89**, 15174 (1988).
7. M. Zhou, C. Huang, V. H. Wysocki, Surface-Induced Dissociation of Ion Mobility-Separated Noncovalent Complexes in a Quadrupole/Time-of-Flight Mass Spectrometer. *Analytical Chemistry* **84**, 6016-6023 (2012).
8. S. Zheng, E. Palovcak, J.-P. Armache, Y. Cheng, D. Agard, Anisotropic Correction of Beam-induced Motion for Improved Single-particle Electron Cryo-microscopy. *bioRxiv*, 061960-061960 (2016).
9. J. A. Mindell, N. Grigorieff, Accurate determination of local defocus and specimen tilt in electron microscopy. *Journal of Structural Biology* **142**, 334-347 (2003).
10. S. H. W. Scheres, RELION: Implementation of a Bayesian approach to cryo-EM structure determination. *Journal of Structural Biology* **180**, 519-530 (2012).
11. E. F. Pettersen *et al.*, UCSF Chimera - A visualization system for exploratory research and analysis. *Journal of Computational Chemistry* **25**, 1605-1612 (2004).
12. P. Emsley, K. Cowtan, Coot: Model-building tools for molecular graphics. *Acta Crystallographica Section D: Biological Crystallography* **60**, 2126-2132 (2004).
13. P. D. Adams *et al.*, PHENIX: a comprehensive Python-based system for macromolecular structure solution. *Acta crystallographica. Section D, Biological crystallography* **66**, 213-221 (2010).
14. M. T. Marty *et al.*, Bayesian deconvolution of mass and ion mobility spectra: from binary interactions to polydisperse ensembles. *Anal Chem* **87**, 4370-4376 (2015).